48th AIAA Aerospace Sciences Meeting Including the New Horizons Forum and Aerospace Exposition
4 - 7 January 2010, Orlando, Florida

Direct Numerical Simulation of Nonpremixed Flame Extinction by Water Spray

P. G. Arias*, H. G. Im†
Department of Mechanical Engineering
University of Michigan, Ann Arbor, MI 48109-2125

P. Narayanan‡, A. Trouvé§
Department of Fire Protection Engineering
University of Maryland, College Park, MD 20742-3031

Abstract

The interaction of turbulent nonpremixed flames with fine water spray is studied using direct numerical simulations (DNS) with detailed chemistry. The study is of practical importance in fire safety devices that operate in the mist regime, as well as an inexpensive temperature control mechanism for gas turbines. The implemented computational methods for the Lagrangian particle-in-cell spray droplet representation and modified characteristic boundary conditions for spray-laden reacting flows are briefly described. The model configuration is a two dimensional ethylene-air counterflow diffusion flame at moderate strain rate. Laminar and turbulent flame simulations are performed with various water loading conditions. Comparison of various simulation cases highlights the flame weakening characteristics due to fluid dynamic strain and water spray evaporation. A modified mixture fraction variable defined in our earlier study [1] is applied to provide correct physical description of the flame response by accurately capturing the flame locations. Findings from this study provide a better understanding of interaction between thermal and aerodynamic quenching in turbulent flame dynamics.

I. Introduction

The advances in high performance computing have allowed for direct numerical simulations (DNS) of laboratory-scale laminar and turbulent flames with complex chemistry without turbulence sub-models. These laboratory-scale laminar and turbulent flame studies can reveal important physical characteristics of fundamental combustion processes in practical devices. Recent combustion DNS studies incorporated advanced multi-physics models to describe soot formation, radiative heat transfer, and spray evaporation, providing temporally and spatially resolved combustion events with detailed information of turbulence-flame interaction characteristics [2-5].

The primary scientific goal of the present study is to understand turbulent flame extinction mechanisms arising from various physical and chemical effects, especially in the presence of fine water spray. The problem is of practical interest in fire safety application, where the utilization of finer water spray is considered a more effective means for flame suppression. As a canonical model problem, we adopt a two-dimensional counterflow nonpremixed ethylene-air flame with spray and turbulent flow injection at the opposing inflow boundaries. Aside from the usual computational challenges associated with combustion DNS, the problem under study has posed additional difficulties. These include correct conservative properties in the implementation of the Lagrangian spray model [6,7] into the Eulerian gas-phase flow solver, and the development of accurate and robust characteristic boundary conditions for reacting flows developed in previous studies [8-13] to account for the effects of spray evaporation.

Therefore, the main scope of the present paper is to describe the improved computational development and implementation for the targeted multi-dimensional turbulent flame-spray interaction simulations. Improvements achieved by the modified approaches are validated by test simulations. Subsequent demonstration of turbulent spray flame simulations is also given and some key results of flame dynamics are briefly discussed.

---

* Graduate Student
† Corresponding author, Email: hgim@umich.edu, Associate Professor, AIAA Associate Fellow
‡ Graduate Student
§ Associate Professor

II. Formulation and Numerical Method

Configuration and Parameters

Figure 1 shows the flame configuration under study. The domain size is 1cm x 2cm with 600x800 grid points in x, y directions. The steady counterflow diffusion flame is initialized first by overlaying the 1-D solution from OPPDIF [14] onto the 2-D dimensional space, and temporally evolving the solution until it reaches a steady state. Improved NSCBC [13] are used for inflows and outflows, with additional modifications described in the next section. The fuel stream is pure ethylene, and the oxidizer stream is air. Initial pressure is 1 atm, and the temperature of the air and fuel streams is 300K. The mean velocities at both inlets are set to 90 cm/s, which yield a corresponding mean strain rate of approximately 180 s^{-1}, a quantity that is about 20% of the extinction strain rate (about 1000 s^{-1} for the flame under study). For the laminar cases, spray droplets are injected at a prescribed velocity close to the local gas velocity at 4 mm from the air side inflow boundary. At the start of the laminar simulations, droplets are injected at discrete time step intervals, simulating different quasi-steady flow rates and thus different prescribed water loadings. For the turbulent simulations, the turbulence field is generated in an auxiliary 2D field using a prescribed energy spectrum, and translated into the time domain using the Taylor hypothesis. The DNS solver, named S3D, employs a 4th order Runge-Kutta time integration and an 8th order central differencing schemes [15]. A reduced ethylene mechanism developed by Lu and Law [16] using 19 major species, 10 quasi steady state species, and 167 reactions is utilized to determine the reaction rates.

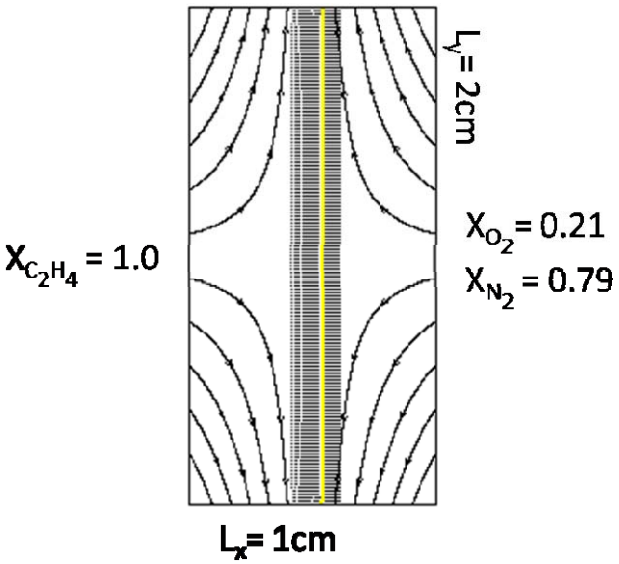

Figure 1. Configuration of counterflow diffusion flame. Solid lines denote potential flow streamlines. Dotted lines represent temperature contours. Solid yellow line indicates the stoichiometric mixture fraction line used as the flame location.

Droplet equations

The spray droplets are treated in a Lagragian formulation [6,7], where the drag force is derived by Stokes law, and the heat conductivity is assumed infinite inside the droplet. The Lagrangian equations of motion for the momentum, mass, and energy can be expressed in the following manner:

$$\frac{dx_{d,i}}{dt} = u_{d,i} \tag{1}$$

$$m_d \frac{du_{di}}{dt} = F_{gd,i} \tag{2}$$

$$\frac{dm_d}{dt} = -2\pi\rho D r_d Sh_d B_M \tag{3}$$

$$\frac{dT_d}{dt} = \frac{4\pi r_d^2}{m_d c_{liq}}\left[\rho \frac{dr_d}{dt} L_{vap} + \frac{\lambda_g (T - T_d) Nu_d}{2r_d}\right] \tag{4}$$

where subscript d indicates droplet properties, and the Sherwood number Sh_d, and Nusselt number Nu_d, and the mass transfer number B_M are defined in Rutland and Wang [7].

Gas Phase Equations

The gas phase equations [6,7] are coupled with the Lagragian droplet equations through additional source terms and are expressed as

$$\frac{\partial \rho}{\partial t} + \frac{\partial}{\partial x_i}(\rho u_i) = \psi_\rho \tag{5}$$

$$\frac{\partial}{\partial t}(\rho u_i) + \frac{\partial}{\partial x_j}(\rho u_j u_i) = -\frac{\partial p}{\partial x_i} + \frac{1}{Re_a}\frac{\partial \tau_{ij}}{\partial x_j} + \psi_{u_i} \tag{6}$$

$$\begin{aligned}\frac{\partial}{\partial t}(\rho e_t) + \frac{\partial}{\partial x_j}\left[(\rho e_t + p)u_j\right] &= \frac{1}{Re_a Pr}\frac{\partial}{\partial x_j}\left(\mu c_p \frac{\partial T}{\partial x_j}\right) + \frac{1}{Re_a}\frac{\partial}{\partial x_i}(u_i \tau_{ij}) \\ &+ \frac{1}{Re_a Sc_n}\sum_{n=1}^{N-1}\left[(h_n - h_{N_2})\frac{\partial}{\partial x_j}\left(\mu \frac{\partial Y_n}{\partial x_j}\right) + (c_{p,n} - c_{p,N_2})\left(\mu \frac{\partial Y_n}{\partial x_j}\frac{\partial T}{\partial x_j}\right)\right] + \psi_e\end{aligned} \tag{7}$$

$$\frac{\partial}{\partial t}(\rho Y_n) + \frac{\partial}{\partial x_j}(\rho u_j Y_n) = \frac{1}{Re_a Sc_n}\frac{\partial}{\partial x_j}\left(\mu \frac{\partial Y_n}{\partial x_j}\right) + \dot{\omega}_n + \psi_\rho \delta_{n,vapor} \tag{8}$$

where the Lagrangian source terms are expressed as

$$\psi_\rho = -\frac{1}{\Delta V}\sum_{k=1}^{n_d}\left(\frac{dm_d}{dt}\right)_k \tag{9}$$

$$\psi_{u_i} = -\frac{1}{\Delta V}\sum_{k=1}^{n_d}\left(F_{gd,i} + \frac{dm_d}{dt}u_{d,i}\right)_k \tag{10}$$

$$\psi_e = -\frac{1}{\Delta V}\sum_{k=1}^{n_d}\left[\frac{d(m_d h_d)}{dt} + F_{gd,i}u_{d,i} + \frac{dm_d}{dt}\left(\frac{1}{2}u_{d,i}^2\right)\right]_k \tag{11}$$

Validation of mass and energy balance

The coupled Eulerian-Lagrangian formulation in the above requires a careful numerical implementation, especially to ensure that all important conservative properties are accurately satisfied. Therefore, some test simulations were conducted by including a single water droplet in a square computational domain in order to assess the global conservation of mass and energy (i.e. integrated across the entire domain), and to check if the d^2-law for droplet evaporation is satisfied. The flow conditions are quiescent, and a single stationary droplet of initial diameter 20 μm at 340 K is placed at the center of a two dimensional domain containing air at 1000 K. The heat from the ambient gas is allowed to evaporate the droplet to completion. The mass and energy of this droplet-gas system are monitored for

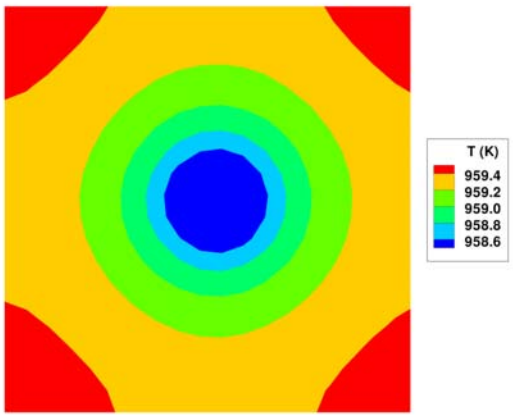

Figure 2. Temperature isocontours for evaporating single droplet. The influence of the droplet spreads radially from the droplet location at the center of the domain.

consistency to satisfy global conservation laws. The droplets are considered completely vanished when their size falls below 1 μm.

Figure 2 shows the temperature isocontours in a two dimensional domain of the size 0.048x0.048 cm^2, with 40x40 grid points to yield 12 μm of grid resolution. The evaporating droplet is seeded at the center of the domain, and the vaporized water spreads radially outwards. A reduction in gas phase temperature is clearly seen as a result of the evaporative cooling.

Figure 3 shows the temporal evolution of the water mass and energy in both liquid and gas phases. During the droplet lifetime of 4.5 ms, the sum of the gas-phase and liquid phase water mass and energy is found to remain constant. Therefore, it is validated that the present numerical approach accurately satisfies the conservation properties.

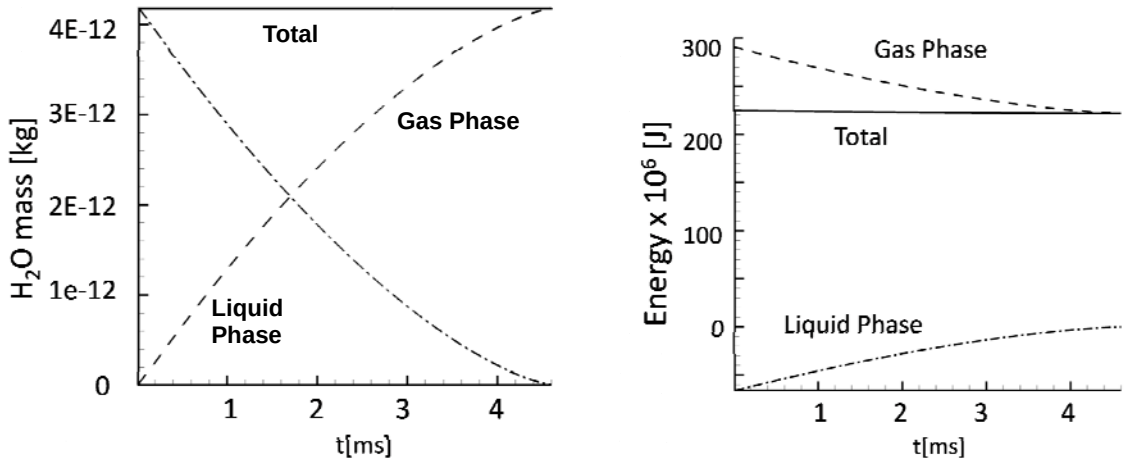

Figure 3. Conservation of water mass and energy in the system. The solid black curve is the total water mass and energy in the system, respectively. On the left, the water mass is expressed as the sum of the liquid water mass (dash-dotted lines) and the gas phase water mass (dashed lines). On the right, the energy is expressed as the sum of the gas phase energy and the droplet energy. The total water mass and energy in the system remains constant over the course of the droplet's lifetime (4.5 ms).

Next, the square of the droplet radius is monitored over the droplet lifetime to verify whether the simulation properly satisfies the well-known d^2-law:

$$r_d^2 = r_{0,d}^2 - Kt \qquad (12)$$

where $r_{0,d}$ is the initial droplet radius and κ is a constant of proportionality determining the droplet lifetime.

The d^2-law behavior is demonstrated in Figure 4 by plotting the square of the droplet's radius, versus time. The behavior of this curve is perfectly linear, demonstrating that the droplet model obeys the d-square law. Therefore, the coupled Lagrangian-Eulerian model employed in the present computational model is validated to yield high-fidelity results for spray-laden reacting flow simulations.

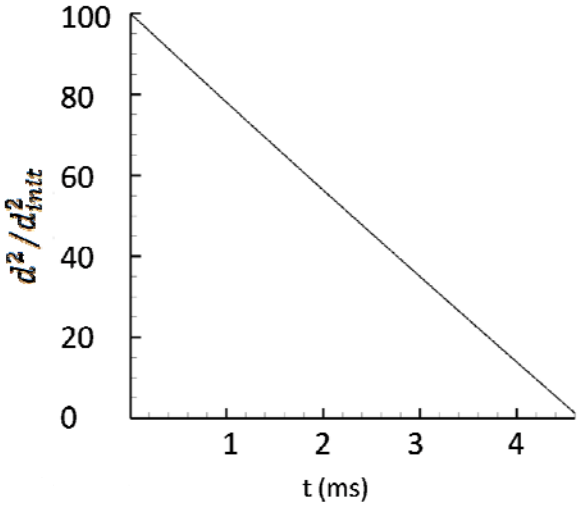

Figure 4. The square of the droplet's radius is plotted over time. The variation is linear, thus showing that the d^2 law is satisfied for the evaporating droplet.

Navier-Stokes Characteristic Boundary Conditions for Spray-Laden Flows

Accurate boundary condition treatment is important in compressible, reacting flows since reflections of acoustic waves at the boundaries can lead to unphysical and significant deviations in the system pressure. This can have adverse effects on the reactions rates of species, and can over estimate the calculated energy release for the given conditions. Since the first development of the Navier-Stokes characteristic boundary conditions (NSCBC) for reacting flows [8], Sutherland and Kennedy [11] was the first to recognize that reactive source terms in the conservation equations must be accounted for in the NSCBC formulation in order to describe the correct acoustic behavior at the boundary. This observation subsequently has led to a comprehensive NSCBC formulation for general boundaries with nonuniform convection, viscous diffusion, and reaction effects [8,9]. In the present application, however, it was recognized that the presence of liquid droplet particles and the associated evaporation events must also be accounted for in the NSCBC treatment.

The incorporation of a Lagrangian particle solver that transfers momentum, mass, and energy from the liquid to the gas phase introduces some unique terms to the source terms in the NSCBC. Since additional sources of momentum, energy, and mass add to the complexity of the gas phase equations, the source terms at the primitive variable have been reformulated and implemented. Following the detailed derivation by Appendix of Sutherland and Kennedy [11], the modified source terms for NSCBC formulation resulting from the droplet evaporation are written as:

$$\begin{bmatrix} s_u \\ s_v \\ s_w \\ s_\rho \\ s_P \\ s_{Y_i} \end{bmatrix} = \begin{bmatrix} \dfrac{\psi_u - u\psi_\rho}{\rho} + \sum_{i=1}^{N} Y_i f_{i,x} \\ \dfrac{\psi_v - v\psi_\rho}{\rho} + \sum_{i=1}^{N} Y_i f_{i,y} \\ \dfrac{\psi_w - w\psi_\rho}{\rho} + \sum_{i=1}^{N} Y_i f_{i,z} \\ \psi_\rho \\ (\gamma-1)\left\{\dfrac{1}{2}\mathbf{u}_\alpha\mathbf{u}_\alpha\psi_\rho - \mathbf{u}_\alpha\psi_{\mathbf{u}_\alpha} + \psi_{e_t} + \sum_{i=1}^{N}\left[-\left(h_i - \dfrac{c_P TW}{W_i}\right)\left(W_i\dot{\omega}_i + \psi_\rho\delta_{i,H_2O}\right) + \rho Y_i f_{i,\alpha} V_{i,\alpha}\right]\right\} \\ \left(\dfrac{1}{\rho}\right)\left(W_i\dot{\omega}_i + \psi_\rho\delta_{i,H_2O}\right) \end{bmatrix} \quad (13)$$

The validity of the new NSCBC formulation was tested in a steady laminar counterflow flames with spray injection. In the test case, air and fuel are injected at the same temperature and pressure conditions as the cases that that were described before. The inflow velocities are 230cm/s, with normal boundary velocity maximums of 1000cm/s. Spray droplets were injected continuously, such that a number of droplets pass through the y-boundary as they vaporize.

To clearly visualize the impact of the new boundary conditions, the simulation was first run with the original (non-spray) NSCBC formulation per Yoo and Im [13], The first step to our validation test was to obtain a steady counterflow diffusion flame for S3D. Next, we injected droplets near the flame on the oxidizer side, leaving the original Navier-Stokes boundary conditions uncorrected to demonstrate the severity of the error on the solution variables. At a later time, the corrected boundary conditions were activated and allowed to recapture the correct, steady counterflow solution, albeit with a diminished flame temperature due to interacting spray.

Figure 5 shows the temporal evolution of the spray run and the affect that uncorrected boundary conditions have on the boundary velocity and pressure. The unphysical accelerations of the normal velocity maximum at the upper open boundary are quite evident when the droplets interact in large quantities, showing a variance of nearly 20% of the steady state value. At around 7.1 ms, we activate the corrected NSCBC, and the flame gas velocity responds immediately to the corrections due to spray source terms. The normal velocity returns to just above 1000cm/s, and the u-velocity profile regains its steady state velocity profile. With the new boundary conditions, we can inject particles without greater confidence that the droplet interaction will not adversely affect the fidelity of the simulation, opening up our ability to test a wide range for later loading conditions and inject turbulence, where there may be a significant amount of droplets that interact and evaporate at the boundary cells.

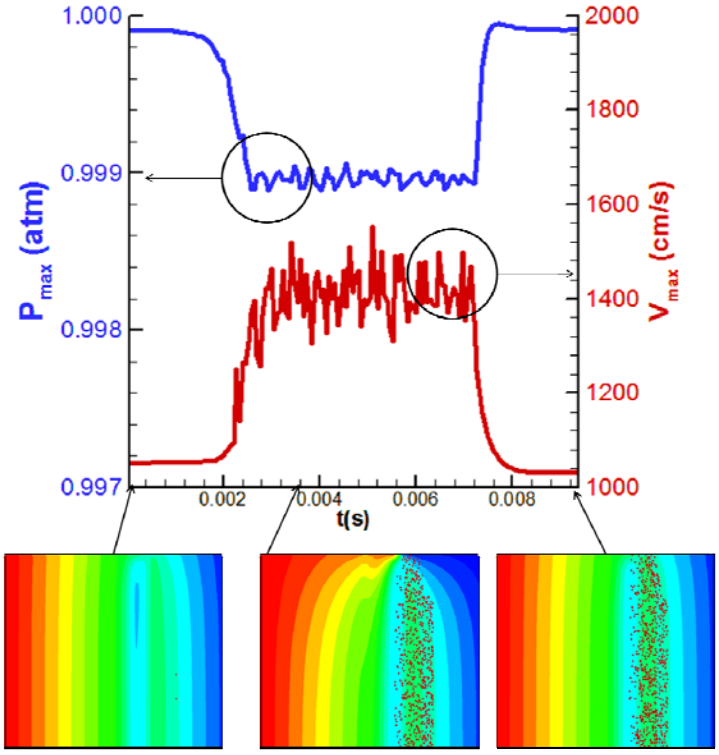

Figure 5. Pressure and normal velocity maximums at upper open boundary. Corresponding u-velocity contours before water interaction (0.05ms), during water interaction with uncorrected NSCBC (3.6ms), and after spray-corrected NSCBC activation (9.3ms). Red dots indicate spray droplets.

III. Results and Discussion

Laminar Flame Simulations

After the fidelity of the simulation was validated, several parametric simulations were conducted with various water loading conditions. The goal of the parametric study is to assess the level of flame weakening by fluid dynamic straining versus that by the spray evaporation.

Table 1 shows the two laminar cases considered in this study. The strain rates fully characterize the initial steady-state volume-integrated heat release rate while the water loading parameter (WLP) is defined as the actual amount of water evaporated normalized by the initial flame power. The case name is designated by the mean strain rate (s^{-1}) and WLP. Case A180-WLP7.5 represents a flame that is only weakened by the amount of water loading, while the A180-WLP18 case leads to flame extinction.

	Strain Rate	Integrated heat release rate	WLP
A180-WLP18	180 s^{-1}	420 kW/m^3	18% (max)
A180-WLP7.5	180 s^{-1}	420 kW/m^3	7.5%

Table 1. Parameters used for two laminar test cases.

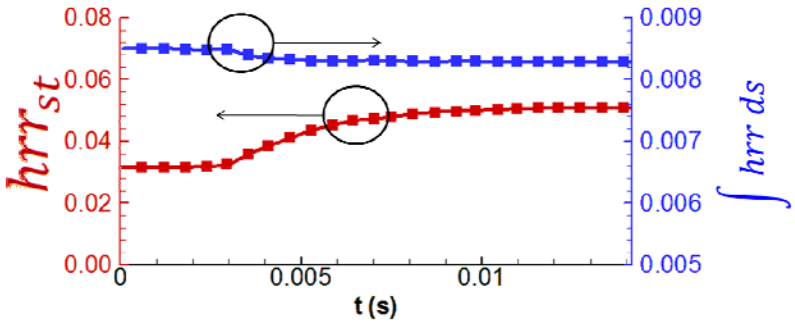

Figure 6. Temporal evolution of the local (red) and integrated (blue) heat release rate for Case A-180-PWL-5.2.

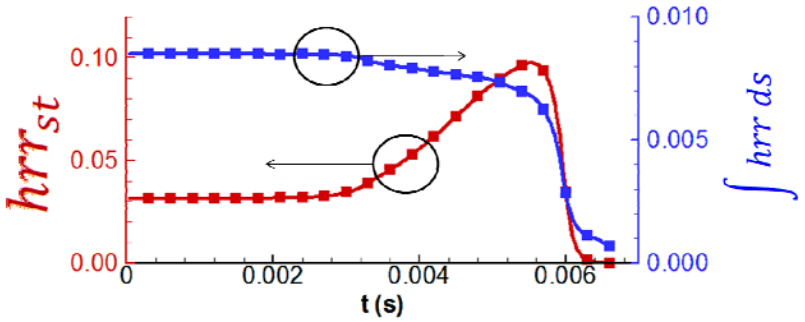

Figure 7. Temporal evolution of the local (red) and integrated (blue) heat release rate for Case A-180-PWL-8.9.

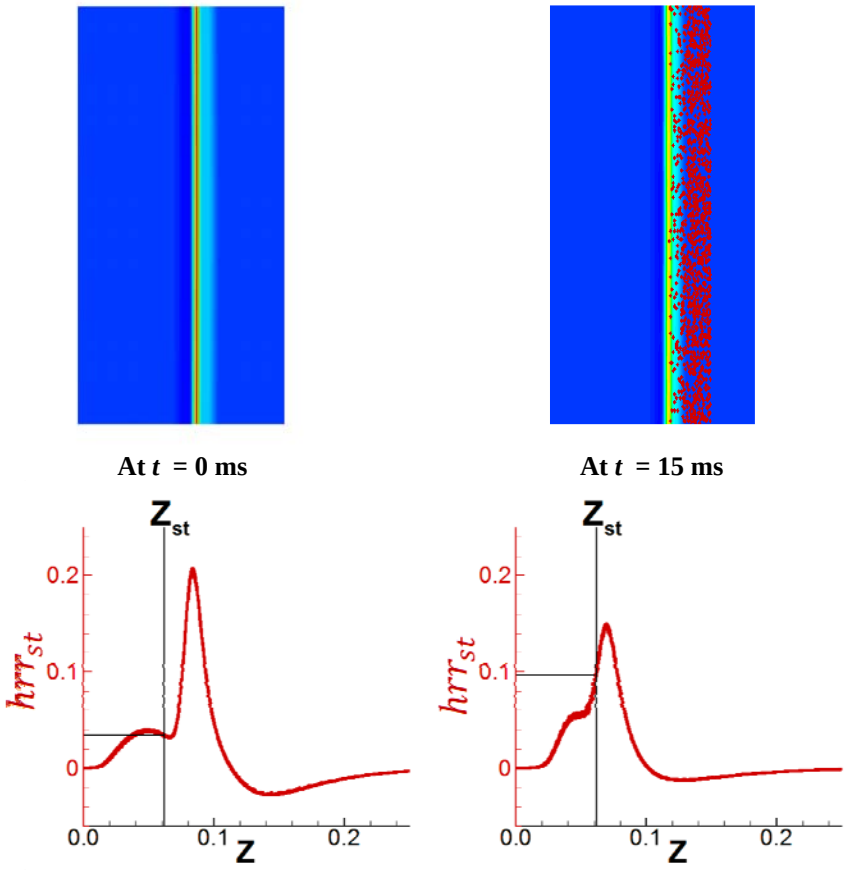

Figure 8. Heat release isocountours (top) and the heat release rate profile across the flame (bottom) for two instants of the simulation at 0 and 12 ms, for Case A180-AWLP5.2. Red dots indicate spray droplets.

Figures 6 and 7 show the temporal evolution of the heat release rate for the two cases. The red curve show the local heat release rate determined at the stoichiometric mixture fraction location at the flame center, while the blue curve shows the heat release rate integrated across the flame norm through the flame center. Figure 8 shows that the heat release rate drops to zero at approximately 6 ms, indicating flame extinction. Note that the local heat release rate appears to increase as the water spray gradually affects the flame (thus weakens the flame), while the integrated heat release rate shows a qualitatively different trend that the heat release rate monotonically decreases in time.

To explain this contradicting behavior, the detailed heat release rate profile across the flame was examined. Figure 8 shows two instantaneous images of the heat release isocontours and the heat release profile across the flame at the beginning of the simulation (0 ms) and after the spray evaporation has been progressed (15 ms), for Case A180-AWLP5.2. It is clearly shown that the overall heat release rate of the flame is decreased by the water evaporation, while the local heat release rate at the stoichiometric mixture fraction (Z_{st}) is seen to increase simply due to the shift in the profile. This suggests that the flame strength is better represented by the integrated heat release rate behavior.

Turbulent Flame Simulations

Test turbulent simulations were performed for spray and non-spray cases in order to demonstrate the qualitative differences between the strain-induced versus the spray-induced extinction behavior in a realistic turbulent condition. Homogenenous isotropic turbulence was injected into the inflow boundaries by first generating in an auxiliary 2D field using a prescribed energy spectrum, with is then translated from the space domain to the time domain by way of the Taylor hypothesis. To observe important extinction or weakening events, the turbulence is applied on an ethylene diffusion flame with an initial mean strain rate of 440 s^{-1}. The spray and the non-spray case are simultaneously performed with the same turbulence field. Our objective in these simultaneous simulations is to show the robust nature of the improved Navier-Stokes Characteristic Boundary Conditions and to show how the droplets interact with the turbulent eddies to accelerate or initiate the formation of flame holes.

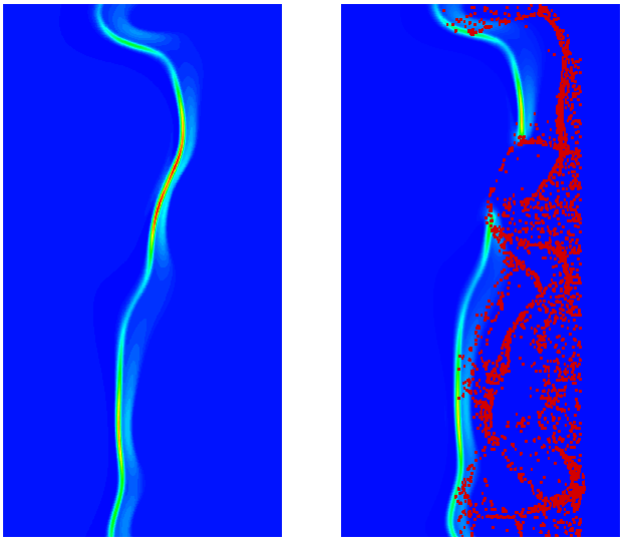

Figure 9. Heat release rate isocontours of turbulent flames without and with spray evaporation, at 4.1 ms.

Figure 9 shows instantaneous images of the heat release isocontours at 4.1 ms, compared between the cases without and with spray (red dots indicate the spray droplets). The initial turbulent flow field is identical for direct comparison. Comparison of two images reveals how droplets interact with turbulence to promote the formation of a flame holes that would not otherwise extinguish. Here the cluttering and organized patterns of spray clouds are the results of the imposed turbulent flow (not shown).

Figure 10 shows four representative instantaneous images of the non-spray turbulent flame during the local extinction event. Figure 11 shows the corresponding distribution of the flame-norm-integrated heat release rate (blue) and the scalar dissipation rate normalized by the steady extinction value along the flame (identified by the stoichiometric mixture fraction isocontour). The scalar dissipation rate is determined in a standard way [17] based on the modified mixture fraction variable [1]. At 4.2 ms, a segment of the flame is weakened by an increased local scalar dissipation rate. Subsequently, local extinction occurs and a flame hole emerges, as evidenced by the suppressed heat release rate in the region. In this particular simulation, the quenched flame hole eventually healed up due to the progressive edge flame speed approaching together.

Figures 12 and 13 show the similar instantaneous images for a spray-induced flame extinction event. During 3.6-3.8 ms, a flame segment subjective to a relatively lower scalar dissipation rate compared to Figure 11 at 4.2 ms is eventually extinguished due to the additional flame weakening effect resulting from the spray evaporation. The resulting flame hole subsequently fails to heal up, again due to the added evaporative cooling, and the two flame

edges are shown to retreat from each other, leading to a widened flame hole and ultimate total extinction. The comparison of Figures 10-11 with Figures 12-13 thus clearly illustrates the complex interaction of fluid dynamic and spray-induced flame weakening that are encountered in a turbulent flame suppression event. While it is only qualitative at this point, it appears that the conventional extinction criterion based on the local scalar dissipation rate is subjected to a significant variation in the presence of additional flame weakening mechanism, such as spray

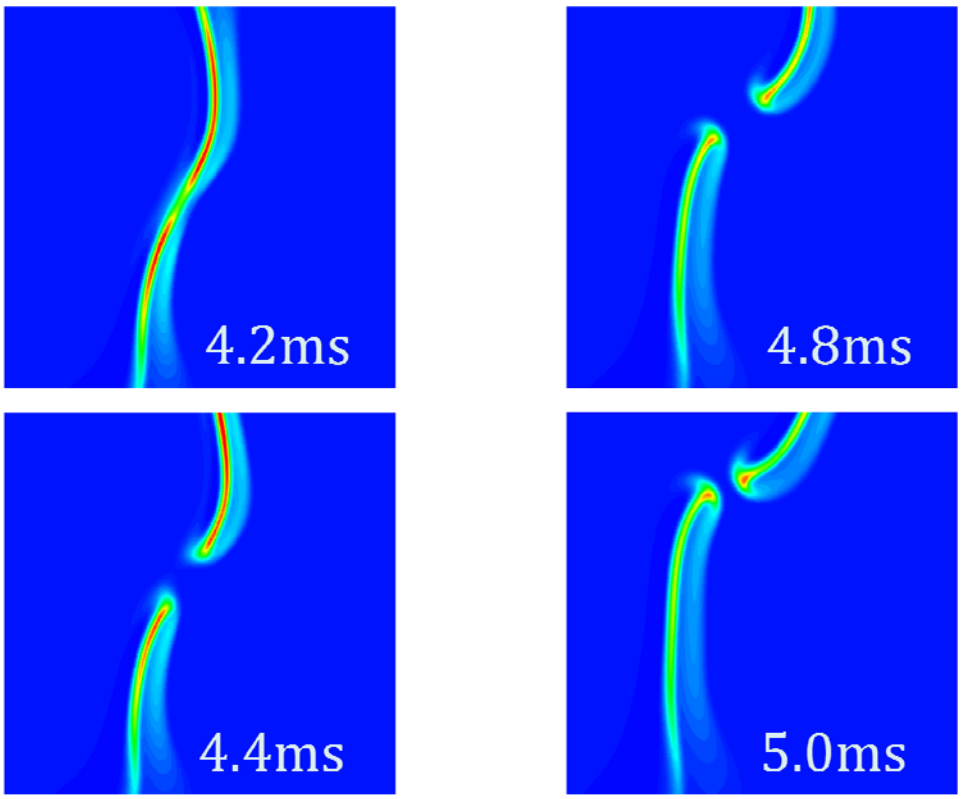

Figure 10. Heat release rate isocontours for the turbulent flame simulation without spray injection.

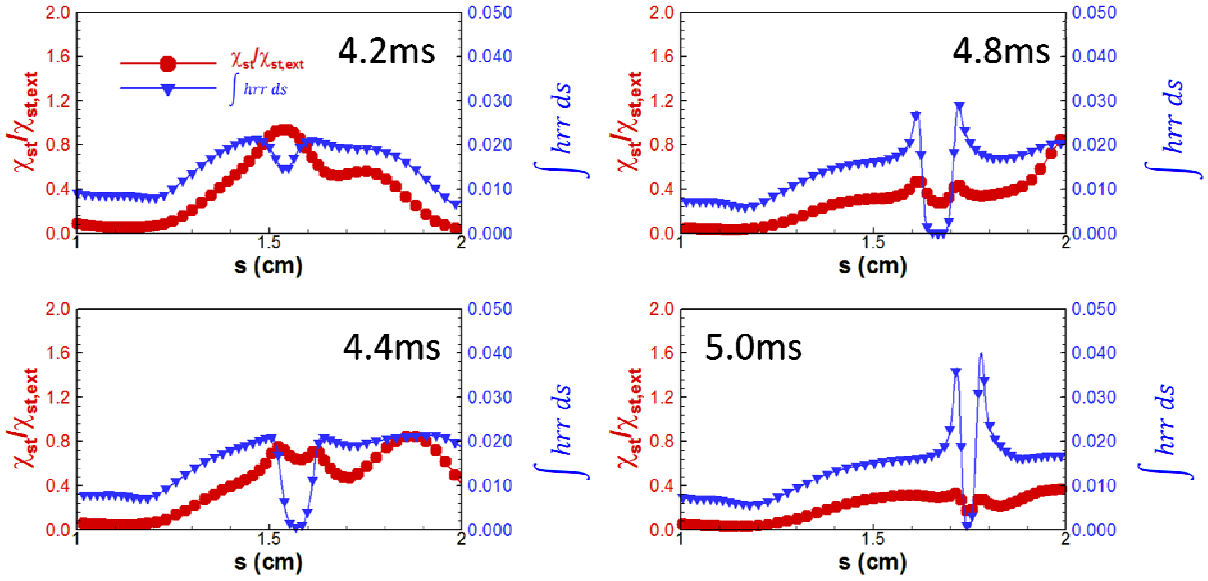

Figure 11. Heat release rate integrated across the flame norm (blue) and the scalar dissipation rate normalized by the steady extinction value (red) for the four time snapshots shown in Figure 11.

evaporation. Further work is underway to identify a possible physical parameter that serves as a unified means to quantify the level of flame weakening, so that a generalized extinction condition can be determined under complex turtulent combustion systems involving multi-physics phenomena.

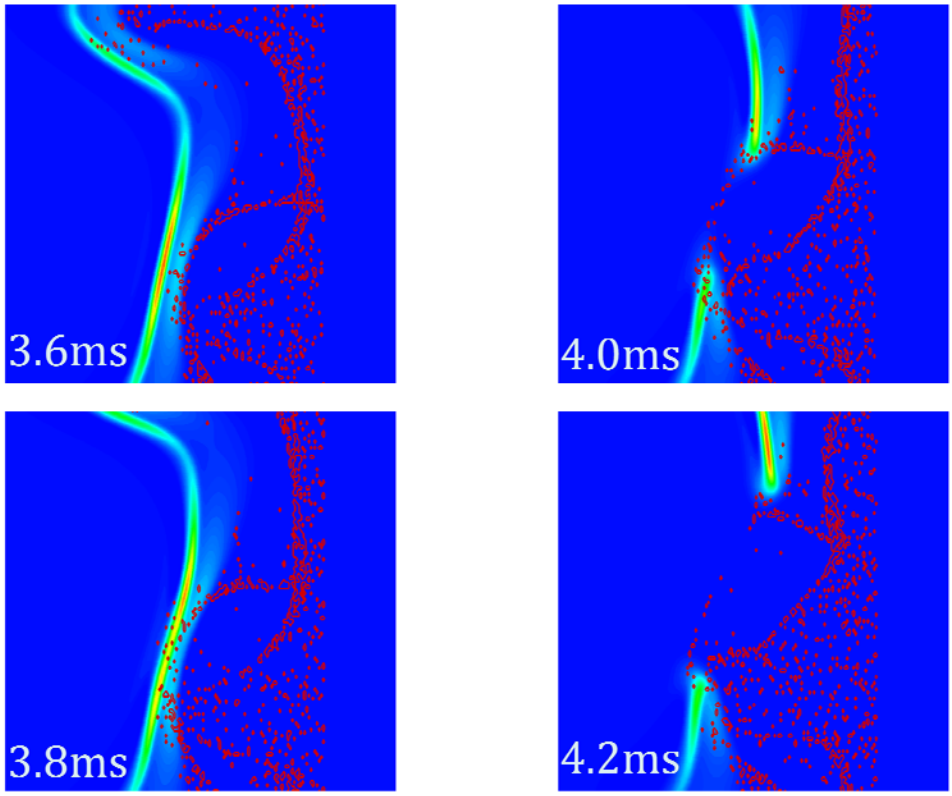

Figure 12. Heat release rate isocontours for the turbulent flame simulation with spray injection.

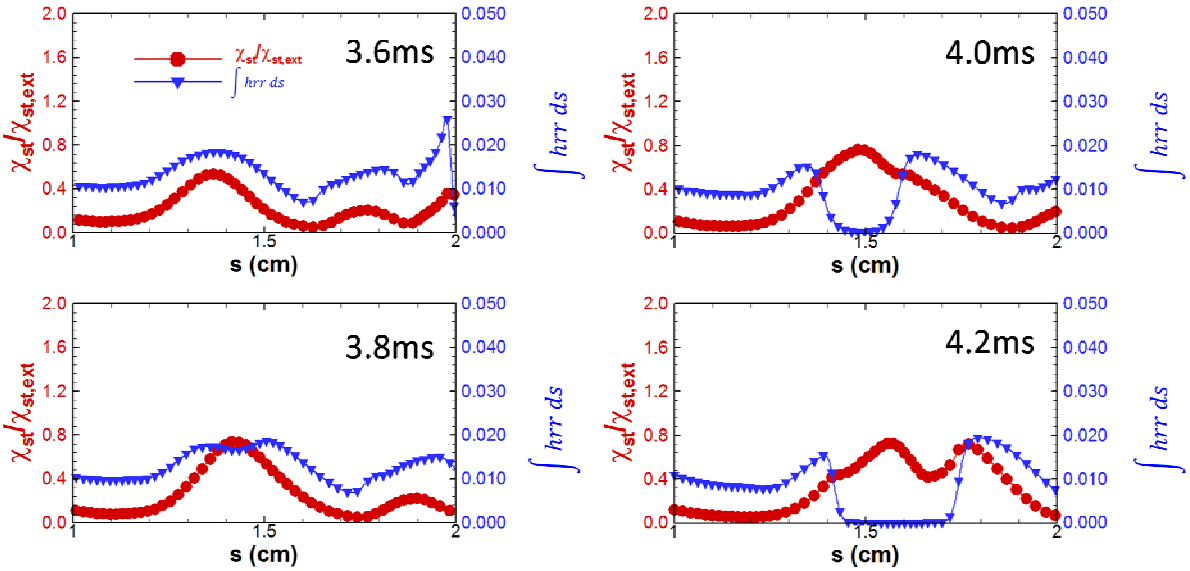

Figure 13. Heat release rate integrated across the flame norm (blue) and the scalar dissipation rate normalized by the steady extinction value (red) for the four time snapshots shown in Figure 13.

IV. Conclusions

Direct numerical simulation of laminar and turbulent diffusion flames in the presence of fine water spray was carried out. The coupling between the Lagrangian liquid droplets and Eulerian gas-phase reacting flows demanded significant efforts towards implementing and validating various computational methods. Important conservation properties of mass and energy have been validated using a single droplet model simulation. A modified Navier-Stokes characteristic boundary conditions were developed and demonstrated to account for the effects of spray evaporation at the computational boundaries such that the fidelity of the simulation was substantially improved.

Laminar flame simulations were conducted with different levels of spray loading. The temporal evolution of the heat release rate revealed a shift in the local heat release rate profile across the flame, such that an appropriate description of the flame intensity requires determination of integrated heat release rate across the flame norm.

Turbulent flame simulations with and without spray injection showed complex interaction between the strain-induced and spray-induced flame weakening effects. Further work is needed to identify and quantify various flame weakening effects, such that a unified extinction criterion may be developed.

V. Acknowledgments

This work was sponsored by Department of Energy, Office of Basic Energy Sciences, SciDAC Computational Chemistry Program.along with the INCITE Program for the computer allocations.

VI. References

[1] P. Narayanan, A. Trouvé, P. G. Arias, H. G. Im, "Mixture fraction and state relationships in diffusion flames interacting with an evaporating water spray," *6th US National Combustion Meeting*, Paper 21I3, May 17-20 (2009).
[2] C.S. Yoo, H.G. Im, "Transient soot dynamics in turbulent nonpremixed ethylene-air counterflow flames," *Proc. Combust. Inst.* **31** (2007) 701-708.
[3] Y. Wang ,C.J. Rutland, "Direct numerical simulation of ignition in turbulent n-heptane liquid-fuel spray jets," *Combust. Flame* **149** (2007) 353-365.
[4] D.O. Lignell, J.H. Chen, P.J. Smith, "Threedimensional direct numerical simulation of soot formation and transport in a temporally evolving nonpremixed ethylene jet flame," *Combust. Flame* **155** (2008) 316-333.
[5] D.O. Lignell, J.H. Chen, P.J. Smith, T. Lu, C.K. Law, "The effect of flame structure on soot formation and transport in turbulent nonpremixed flames using direct numerical simulation," *Combust. Flame* **151** (2007) 2-28.
[6] Y. Wang, C. J. Rutland, "Effects of temperature and equivalence ratio on the ignition of n-heptane fuel droplets in turbulent flow," *Proc. Combust. Inst.*, **30** (2005) 893-900.
[7] Y. Wang, C. J. Rutland, "Direct numerical simulation of ignition in turbulent n-heptane liquid fuel spray jets," *Combust. Flame*, **149** (2007) 353-365.
[8] T.J. Poinsot, S.K. Lele, "Boundary conditions for direct numerical simulation of compressible viscous flows," *J. Comp. Phys.* **101** (1992) 104-139.
[9] M. Baum, T.J. Poinsot, D. Thevenin, "Accurate boundary conditions for multi component reactive flows," *J. of Comp. Phys.* **116** (1994) 247-261.
[10] N. Okong'O, J. Bellan, "Consistent boundary conditions for multicomponent real gas mixtures based on characteristic waves," *J. of Comp. Phys.* **176** (1994) 330-334.
[11] J.C. Sutherland, C.A. Kennedy, "Improved boundary conditions for viscous, reacting, compressible flows," *J. of Comp. Phys.* **191** (2003) 502-524.
[12] C.S. Yoo, Y. Wang, A. Trouve, H.G. Im, "Characteristic boundary conditions for direct simulations of turbulent counterflow flames," *Combust. Theory and Modeling* **9** (2005) 617-646.
[13] C.S. Yoo, H.G. Im, "Characteristic boundary conditions for simulations of compressible reacting flows with multi-dimensional viscous and reaction effects," *Combust. Theory and Modeling* **11** (2007) 259-286.
[14] A.E. Lutz, R.J. Kee, J.F. Grcar, F.M. Rupley, "OPPDIF: a Fortran program for computing opposed flow diffusion flames," Sandia National Laboratories, Report SAND96-8243, 1996.
[15] H.G. Im, A. Trouvé, C.J. Rutland, J.H. Chen, Terascale high-fidelity simulations of turbulent combustion with detailed chemistry, DOE SciDAC Program, 2001-2008
[16] T. Lu, C.K. Law, "A directed relation graph method for mechanism reduction," *Proc. Combust. Inst.* **30** (2005) 1333-1341.
[17] N. Peters, *Turbulent Combustion*, Cambridge University Press, Cambridge, UK (2000).